The Analysis of Losses in High-Power Fault-Tolerant Machines for Aerospace Applications

Glynn J. Atkinson, *Member, IEEE*, Barrie C. Mecrow, *Member, IEEE*, Alan G. Jack, *Member, IEEE*, David J. Atkinson, Parminder Sangha, and Maamar Benarous

Abstract—This paper discusses the design of a fault-tolerant electric motor for an aircraft main engine fuel pump. The motor in question is a four-phase fault-tolerant motor with separated windings and a six-pole permanent magnet rotor. Methods of reducing machine losses in both the rotor and stator are introduced and discussed. The methods used to calculate rotor eddy current losses are examined. Full three-dimensional finite-element (FE) time stepping, two-dimensional (2-D) FE time stepping, and 2-D FE harmonic methods are discussed, and the differences between them and the results they produce were investigated. Conclusions are drawn about the accuracy of the results produced and how the methods in question will help the machine designer.

Index Terms—Aerospace industry, electromagnetic performance, fault tolerance, high specific output, losses, modeling, permanent-magnet (PM) machines, simulation.

I. INTRODUCTION

AN INTEGRATED electric main engine fuel pump in an aircraft has a number of potential benefits. The fuel control system will be lighter in weight, smaller, simpler, and more efficient than conventional systems using a mechanically driven pump. Fuel flow within the engine can be matched precisely to the engine's operating conditions, rather than governed solely by the engine speed.

Previous research by a variety of authors [1]–[11] has been carried out on the concepts, development, building, and testing of fault-tolerant drives. The authors have developed a 16-kW 15 000-r/min four-phase six-pole permanent-magnet (PM) fault-tolerant electric drive, which has been tested on a main engine fuel pump [12]. This system is illustrated in Fig. 1. Each of the four phases is driven by a sinusoidal current supplied by a separate single-phase H-bridge converter. The machine design ensures magnetic, electrical, mechanical, and thermal isolation between phases. It runs flooded in aircraft fuel, which acts as an excellent coolant, permitting a very high electrical loading.

The next stage of research has concentrated on increasing the power and speed of this machine to 100 kW and 20 000 r/min
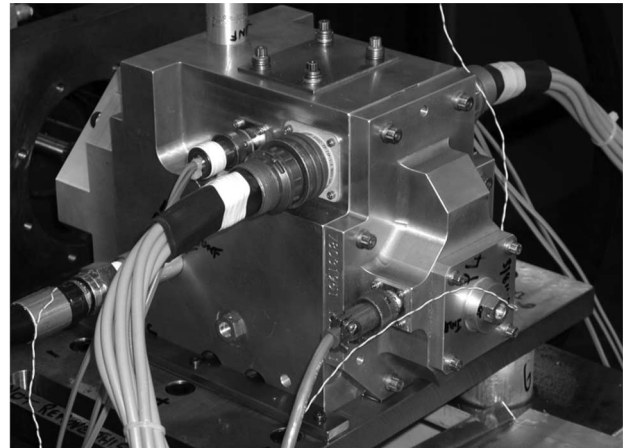
Fig. 1. 16 kW fault-tolerant electric motor on a test bed.
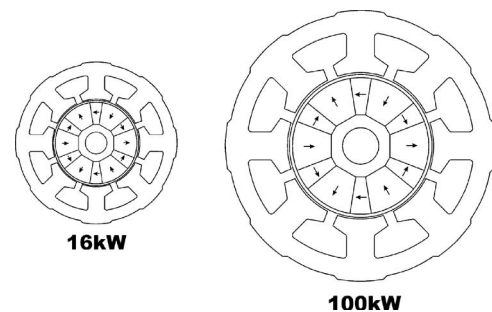

16kW

100kW

Fig. 2. Comparison between the 16- and the 100-kW fault-tolerant motors.

[13]. This power level has been identified for a medium- to large-sized aircraft. An initial design, which is based on the 16-kW machine, held constant the magnetic and electrical loadings while increasing the physical size of the machine to provide enough volume to meet the increase in torque. A scale comparison of the two machines is given in Fig. 2.

Some prior knowledge of the losses to be expected in the 100-kW machine was required. To achieve this, a series of models were created to calculate no-load loss (iron loss and viscous drag loss), full-load winding loss, and full-load rotor eddy-current loss. On calculating these losses, it has become evident that, when compared to the measured losses for the 16-kW machine, the efficiency of the 100-kW machine will decrease, and a change will occur in the balance of machine losses. Rotor eddy-current loss becomes the dominant loss mechanism, contributing 40% of the total loss. These results are presented in Table I.

TABLE I
LOSSES FOR A 16- AND A 100-kW MACHINE

Loss Mechanism	Loss as a percentage of output power	
	16kW machine	100kW machine
Full-load rotor loss	1.6%	7.9%
No-load losses	1.9%	7.5%
Full load winding loss	3.4%	4.4%
Total machine loss	**6.9%**	**19.8%**

Having found that the model's rotor eddy currents are the dominant source of loss, it has been necessary to seek ways to minimize this loss. In order to do that, a simplified analysis method has been developed. This allows reasonable fidelity while at the same time indicating the dominant loss making harmonics and is very simple to apply at the design stage. The simplified model is compared with both two-dimensional (2-D) and three-dimensional (3-D) time-stepped models with moving rotors, which highlights problems implicit in the apparently more rigorous methods.

II. DESIGN MODIFICATIONS TO REDUCE LOSS

The move to larger power output fuel pump motors has resulted in a change in the amount and balance of losses, with rotor loss becoming dominant. Overall total machine losses have increased as a percentage of output power from 6.9% for a 16-kW machine to 19.8% for a 100-kW machine. Considerable effort has gone into designing a 100-kW machine with a more acceptable efficiency. The steps taken to achieve this are discussed in this section of this paper.

A. Rotor Eddy Current Loss

Nonsynchronous air-gap magnetic fields induce eddy currents in the rotor. The loss due to these is significant for the following two reasons.

1) Each slot contains only one nonoverlapping winding to ensure that magnetic, electrical, and thermal isolation is maintained to provide fault tolerance. This isolated winding arrangement results in a square air-gap magnetomotive force (MMF) profile and, consequently, a high degree of nonsynchronous air-gap harmonics.
2) The rotor is made using samarium cobalt magnets retained by a nonmagnetic steel sleeve to withstand the centrifugal force of the magnets at high speed. Both of these materials are electrical conductors.

For simplicity of explanation, the two-pole field will be considered as "the fundamental." This means that the "third harmonic" is the six-pole field, which is the desired component to produce the torque. This avoids the confusion of sub- and superharmonics.

The air-gap harmonic spectrum can be altered by changing the stator design. The tooth pitch can be modified to increase the magnitude of the torque-producing six-pole field while decreasing the magnitude of the majority loss-inducing fifth harmonic [12]. Fig. 3 illustrates the original stator design with equal wound and spacer tooth span and the altered design for which a reduction of 29% in rotor eddy-current loss has been calculated.
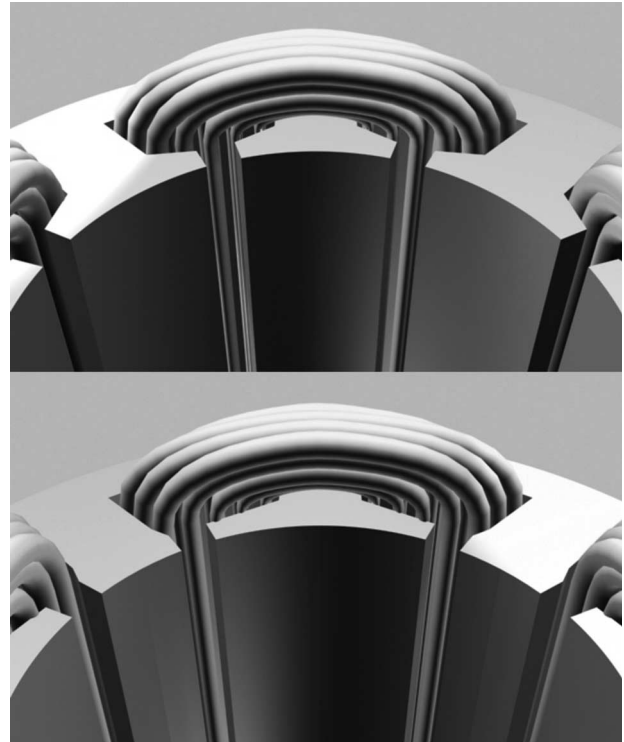

Fig. 3.   Original and new stator design.

The choice of magnet is somewhat limited by the thermal requirement of the machine, and the high centrifugal forces and harsh machine environment limit the choice of rotor sleeve.

Rotor eddy-current loss (particularly due to the high-order harmonics) can be reduced by increasing the air-gap length. This effectively reduces the depth to which the high-order harmonics penetrate into the rotor, reducing the loss due to them. However, one must compensate for the reduction in air-gap flux density by increasing phase turns and/or current. There would seem to be an optimum point at which reductions in high-order rotor loss and viscous drag due to the increased air-gap size are offset by an increase in low-order rotor loss and winding loss due to the increased air-gap MMF required to maintain output power.

B. Winding Loss

On increasing the size, output power, and speed of the fault-tolerant machine, the number of turns has been reduced, when operating at the same supply voltage. Fewer but larger diameter conductors result in increased skin and proximity effects. Winding loss at full load and speed is now 4.4 kW, which is seven times the equivalent dc winding loss. (Table II).

Adoption of the new stator design (Fig. 3) encourages leakage flux to spread more into the slot, as shown in Fig. 4. This increases proximity loss. Along with this, the air-gap length has been increased to reduce rotor eddy-current loss. This reduces magnetic loading, which requires an increase in electrical loading to maintain the same output power, further exacerbating the problem. Hence, 7 kW of loss results (Table II).

With multistranded Litz-type wire, which consists of 15 bundles of ten-strand conductors, a reduction in total winding

TABLE II
REDUCING WINDING LOSS

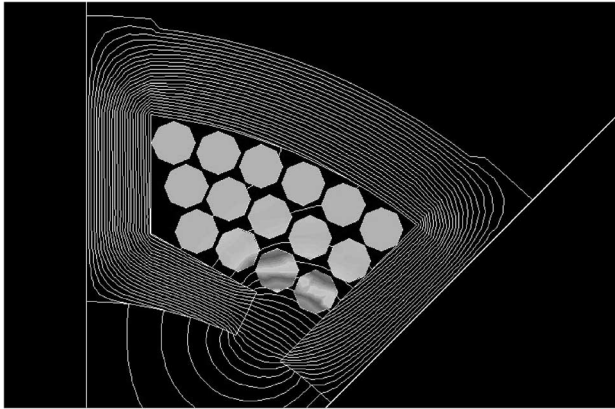| Winding type, Stator design	DC Loss (W)	Total Winding AC Loss (W)	Ratio of Total AC Loss To DC loss
12 Solid Conductors, Original stator design	621	4419	7.11
15 solid conductors, New stator design	1323	7083	5.35
15 ten-strand conductors, New stator design	2065	2492	1.21

Fig. 4.   2-D FE simulation of winding loss using the new stator design.

loss from 7 to 2.5 kW occurs. As shown in Table II, the ac loss is now only 21% greater than the dc loss.

C. No-Load Loss

A series of tests carried out on the 16-kW machine have separated winding loss, rotor eddy-current loss, and no-load loss [12]. As the name suggests, no-load loss is measured with the machine unloaded and open circuit, being driven by an external motor. The loss measured consists of viscous drag, stator iron, and bearing loss.

The machine is fuel cooled by running the machine flooded with fuel. Fuel in contact with the rotor surface imposes a viscous drag loss on the machine. As shown in (1), the drag torque M is related to the axial length l_a, the rotor outside diameter r, the speed ω, and the viscosity of the fuel ρ. The flow of fuel is turbulent, with a high Reynold's number. Consequently, the coefficient of friction as shown in [14] is given by (2) with an air-gap length l_g and kinematic viscosity μ. That is,

$$M = 0.5 C_m \pi r^4 l_a \rho \omega^2 \qquad (1)$$

$$C_m = \frac{0.146 \times \sqrt[4]{l_g \frac{R_o}{R_i}}}{\sqrt{(\rho \times \omega \times r \times l_g / \mu)}}. \qquad (2)$$

For the 100-kW machine at 20 000 r/min, drag loss comprises 84% of the no-load loss. This is reduced by decreasing the rotor outside diameter and, in turn, increasing the air-gap length, which also reduces the rotor eddy-current loss. As drag loss is most heavily influenced by the rotor diameter, a reduction in

TABLE III
LOSSES FOR A 16- AND A 100-kW MACHINE

Loss Mechanism	Loss as a percentage of output power	
	100kW initial design	100kW improved design
Full-load winding	4.4%	2.5%
No-load	7.5%	5.6%
Full-load rotor	7.9%	6.0%
Total	19.8%	14.1%

rotor diameter from 76.8 to 70 mm results in a reduction in drag loss from 6.4 to 4.5 kW, which is a 30% reduction.

The most obvious way to reduce iron loss is to use a thinner lamination steel. When 0.35-mm laminations are used, the iron loss is only 5.7% of the total loss for this machine, and decreasing the lamination thickness to 0.1 mm will only shave a further 2.3% off the total loss. The increased cost associated with thinner laminations far outweighs the benefits of reducing total loss by such a small amount.

D. Total Machine Loss

As shown in the previous sections, reducing loss due to one mechanism can result in an increase in loss due to the others. The designer must find the best compromise of the methods available to reduce the total loss. The initial design is improved by reducing the rotor diameter, increasing the air-gap length, changing the stator tooth span, and using multistrand conductors. This causes a reduction in no-load, winding, and rotor eddy current losses from 19.8% of output power to 14.1%, as shown in Table III.

III. DISCUSSION OF MODELING ISSUES

As can be seen, rotor eddy currents are still the dominant source of loss, and hence, significant effort in their calculation is worthwhile.

In researching suitable methods, it is very useful for the designer to devise techniques that yield insight into the sources of loss. This mitigates against time-stepping techniques with moving rotors, which tend to lead to a single composite answer. It is also clear that reducing the designer's effort in obtaining solutions permits greater experimentation and, hence, better designs. At the same time, the methods employed must have sufficient accuracy. The authors' studies show that it is possible to get very inaccurate answers using full 3-D time-stepping models simply by using inadequate mesh subdivision near tooth tips.

IV. ROTOR EDDY-CURRENT LOSS—TIME-STEPPING APPROACH

A. 3-D Modeling

Full knowledge of the time-varying magnetic field distribution within the machine requires the use of 3-D time-stepping finite-element (FE) methods with movement incorporated into the mesh. Significant portions of the rotor loss result from small geometrical details such as the shape of the slot opening, and hence, fine discretization is required in these areas for an accurate result. The resultant problem is exceptionally large and
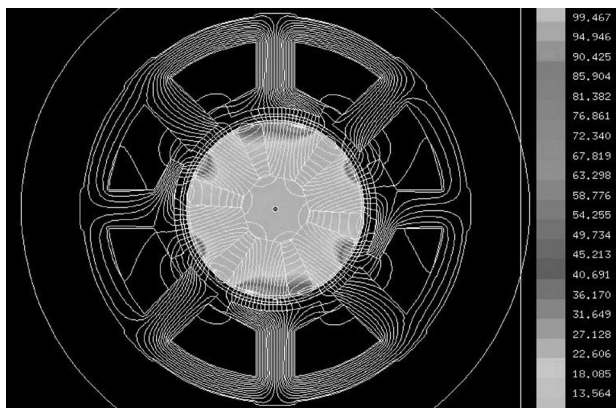
Fig. 5. Flux and loss contour plot produced for the 100-kW machine using the time-stepping method.
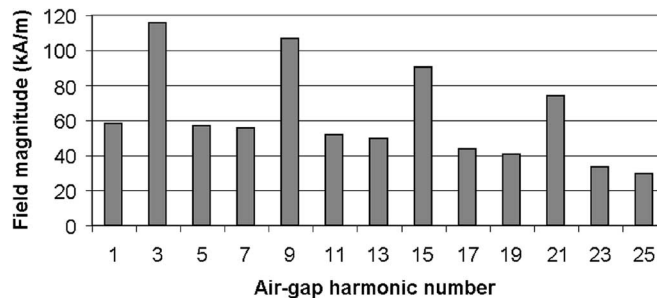

Fig. 6. Air-gap tangential magnetic field spectrum of the 100-kW machine.

Fig. 7. 2-D FE model of the 15th harmonic applied to a section of the rotor.

takes several days of computation to achieve a single solution. For this reason, it is not a preferred design method, except for final design verification. Approximations are generally made to reduce the model complexity.

B. 2-D Modeling

If the end effects are not significant, then rotor eddy-current loss, along with other electromagnetic effects, can be calculated using 2-D FE software, in which time-stepping is used in conjunction with moving surfaces. A 2-D FE model of the 100-kW machine was built with a rotating rotor, PM excitation, nonlinear stator iron, and sinusoidal winding currents. The model was set to run over four electrical cycles with 40 time steps per electrical cycle. The first cycle allows the solution to settle, and the last three represent one complete mechanical revolution. A full field solution is produced at each time step. Fig. 5 illustrates an example instantaneous flux distribution with rotor eddy-current loss density superimposed via shading.

Both instantaneous and time-domain results can be obtained for rotor eddy-current loss, flux density at a position, magnetic field strength on a surface, and output torque. Rotor eddy current loss is made up of both loss due to the MMF asynchronous harmonics and loss due to flux perturbations caused by the magnets moving beneath a slot opening and then a tooth.

V. ROTOR EDDY-CURRENT MODELING—HARMONIC APPROACH

An alternative approach to this all-in-one method is to analyze rotor eddy-current loss using a simplified harmonic approach. Rotor eddy-current loss is due to changes in the air-gap magnetic field. When viewed from the rotating rotor, this field is alternating in both time and space and has a complex waveform. The harmonic approach sums the effect of each individual harmonic as seen from the rotor.

The air-gap tangential magnetic field strength is defined by the rate of change of MMF with respect to position. The peak magnetic field occurs at the slot openings where the tangential magnetic field strength is the greatest and is virtually zero elsewhere. The harmonics of this field are found by Fourier
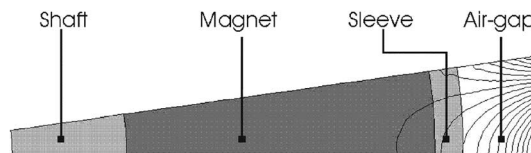
decomposition. This operation gives the air-gap harmonic spectrum shown in Fig. 6.

Torque is produced by the interaction of the six-pole rotor and stator fields, or the third air-gap harmonic. This torque-producing harmonic is locked onto the rotor and, as such, induces no rotor eddy-current loss. All other harmonics are asynchronous with the rotor and rotate alternately backward and forward, producing ever-increasing frequency fields in the rotor. It is the eddy-currents induced with these asynchronous fields that cause the rotor eddy-current loss that has become an issue with this type of machine.

In an interesting approach adopted in [15]–[17], an analytical solution based upon a similar harmonic approach has been developed. However, for this application, the range of design options included harmonics that produced significant eddy current reaction, and hence, the analytical method of [15]–[17], which neglects eddy current reaction, is not appropriate. The authors were also examining segmentation schemes for the magnet assembly for which analytical solutions are more difficult and, therefore, chose to adopt a 2-D FE approach to the solution.

A 2-D FE simulation was carried out, with each harmonic of the air-gap tangential field applied as a current sheet on the surface of the stator bore. Using periodic boundaries, only a small section of the rotor needs to be modeled. Fig. 7 illustrates this for the fifteenth harmonic.

The 2-D FE model of the rotor segment with field applied was solved for a known field strength. The bulk of the eddy-currents occurs within the magnet and the sleeve, which have linear magnetic permeability. Eddy-current loss is, consequently, proportional to the field magnitude squared, so eddy-current loss can be calculated for any field magnitude with this scaling factor once a set of results with a known field magnitude has been generated. The effect of changes in electrical loading can then be found without running a new FE simulation. Changes to the tooth span and slot opening of the stator, which affect only the harmonic spectrum, can also be investigated by applying the correct magnitude for each
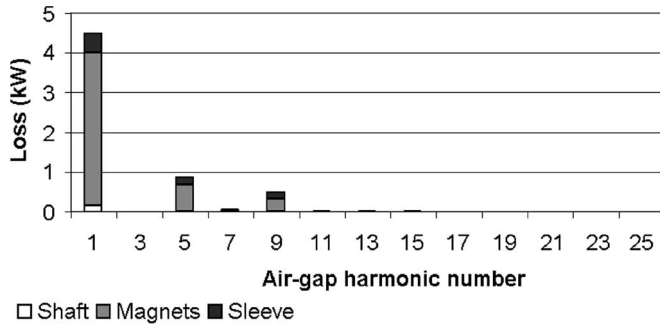
Fig. 8.   Rotor eddy-current loss spectrum.

TABLE IV
ROTOR EDDY-CURRENT LOSS CALCULATED VIA A HARMONIC
AND A TIME-STEPPING APPROACH

Source of loss	Finite element calculated loss in Watts		Percentage difference
	Harmonic method	Time step method	
Magnets	4937	4488	-9%
Sleeve	904	824	-9%
Shaft	143	67	-53%
Total loss	5984	5379	-10%

harmonic. This allows many changes in design to be analyzed very quickly.

Changes in rotor or stator diameter, air-gap size, rotational frequency, and rotor materials will require a new FE model to be built and simulated, which is a quick process for such a small model. When the 2-D FE simulation was carried out and the correct magnitude for each harmonic applied, the rotor eddy-current loss spectrum shown in Fig. 8 was produced. This spectrum allows the principal source of loss to be identified.

The majority of loss is due to eddy currents induced by the first harmonic (i.e., the two-pole field). This was not the case, however, for the original 100-kW machine design based on the 16-kW machine's design. With the original stator tooth layout and slot opening size, the majority of rotor eddy-current loss was due to the fifth air-gap harmonic (i.e., the ten-pole field) [13]. This information indicated that a redesign of the stator tooth width was required to reduce the excessive rotor losses. The effect of this change was found by simply producing a new Fourier series and applying the magnitude of each harmonic to the already-generated FE results with the scaling factor applied to take account of the difference between the simulated and actual harmonic field magnitude. This procedure indicated a 13% reduction in total rotor eddy-current loss and an increase in machine torque. With the electrical loading dropped to bring the torque back to its rated value, the reduction in rotor eddy-current loss became 29%. This change to the machine design is revealed by the harmonic method but would not be so evident with the time-stepping approach.

VI. COMPARISON BETWEEN HARMONIC AND TIME-STEPPING APPROACHES

The same machine design has been simulated at full speed and full load using the two methods described. Table IV summarizes the amount of rotor eddy-current loss calculated by each method.
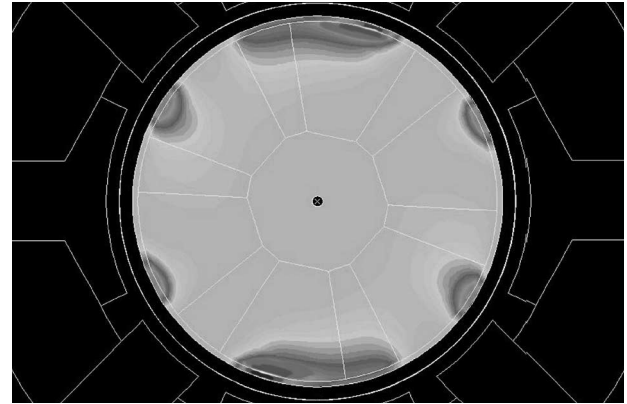

Fig. 9.   Rotor eddy-current shade plot. Dark region indicates high loss density.

A 10% difference exists, with the time-stepping method providing a lower value for the total loss when compared to the results from the harmonic method. This difference is investigated in the following sections.

A. Rotor Loss Composition

The harmonic loss method revealed that the majority of rotor eddy-current loss is due to the 1st harmonic (2-pole asynchronous field). This can also be seen in the results from the time-stepping method as shown in Fig. 9. This is a shade plot of rotor eddy-current loss density. A diametrically opposite region of high loss can be seen in the rotor. Since these regions are 180 degrees apart, the high loss region must be due to the 1st harmonic.

B. Effect of Nonlinearity

In the time-stepping model, the stator iron is modeled with a $B-H$ curve to represent nonlinearity, whereas in the harmonic method, the stator iron is assumed infinitely permeable.

There will be an MMF drop in the core, which has not been taken into account in the harmonic method. To consider this effect, the time-stepping model was run with a linear and very high permeability stator. A slight increase in rotor loss from 5379 to 5459 W was found when compared to the nonlinear case. Clearly, saturation of the stator does not have a significant impact upon rotor eddy-current loss.

C. Harmonic Spectrum

The harmonic approach uses the Fourier series calculated for the idealized case, where the tangential field strength is assumed to be constant across each stator slot opening and zero across each tooth. This profile is shown in Fig. 10. It is of interest to compare this idealized field profile with that obtained from the slot in the time-stepping model.

With the magnets demagnetized, as is the case in the harmonic method model, the magnetic field strength profile generated by the time-stepping approach is spread beyond the slot and has a lower magnitude than the idealized case. This spreading is due to the limited amount of elements placed in
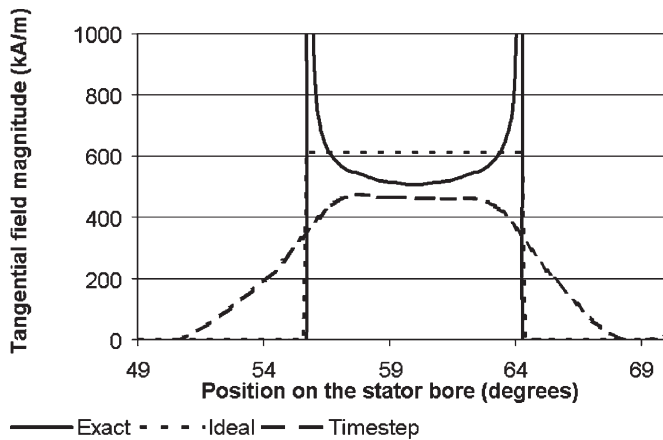
Fig. 10. Tangential field profile at the slot opening.

Fig. 11. Total loss against time with the magnets on.

Fig. 12. Total loss against time with the magnets off.

the region of the slot, i.e., it is an error in the analysis rather than a real effect.

For the restricted case where the stator iron is assumed infinitely permeable, an "exact" solution is shown in Fig. 10 (this can be derived analytically or using a magnetostatic model of the slot with many elements in the slot and infinitely permeable iron). The "exact" solution shows how the tangential H field tends toward infinity close to the tooth corners. The idealized case adopted by the harmonic model is closer to the "exact" case than that taken from the time-stepping model, simply because the time-stepping model does not contain enough elements to give an acceptably accurate model.

The smoothed profile from the time-step model does not adequately model the high-order harmonics. This was calculated to be the principal reason why the time-stepping method predicted lower losses. It also suggests that the harmonic method is more accurate.

D. Tooth Ripple Loss Within the Total Eddy-Current Loss

Tooth ripple loss occurs because of rotor flux perturbations caused as the magnets pass beneath a slot opening and then a tooth. This effect is implicitly included when using a time-stepping method as the magnets, slots, teeth, and movement are all included in the model. Tooth ripple loss can be separated from the total MMF harmonic losses by running the simulation with the currents turned off. All eddy-currents are then due to this flux perturbation, or tooth ripple as it is often known. For a machine such as the one described here, the large air-gap (5 mm) results in small mean ripple loss of 44 W. The tooth ripple effect produces a varying loss with time, as illustrated in the full-load time-stepping result in Fig. 11. By way of a comparison, the model was also run with the magnets demagnetized, thus removing the tooth ripple loss but still retaining the loss due to stator harmonics. Fig. 12 illustrates how the varying loss is removed, and the result settles into a constant loss as expected.

E. Magnet Segmentation

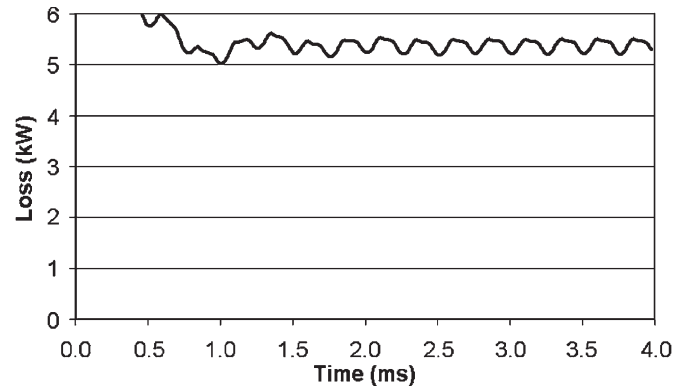The fields shown in Figs. 5, 7, and 9 are examples with non-insulated magnets, akin to a solid annular ring. However, it is possible to deliberately insulate between the separate magnets and even further subdivide the magnets with separating insulation. This magnet segmentation may act to reduce overall loss and, hence, needs consideration. Without explicit insulation, it is likely that the contact resistance between segments is rather small in comparison to the effective magnet resistance. To consider segmentations 2, 3, and 4, insulated magnet segments per pole have been considered. To represent the limiting case, zero-conductivity magnets have also been considered. Insulated magnet segments have been found to significantly reduce eddy-current loss in cases without a conducting sleeve [15], however, its inclusion somewhat complicates the situation.
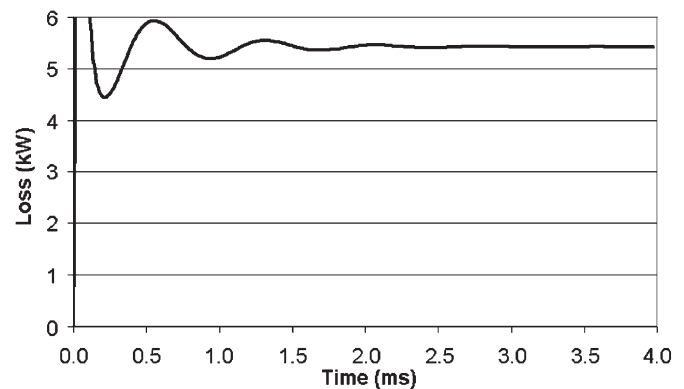
The total eddy current reaction MMF is shared between the sleeve, magnets, and shaft. On taking into account magnet segmentation, losses in the magnets are indeed shown to be reduced (i.e., 10% for two segments per pole and 25% for four). However, the sleeve reaction MMF is increased due to the reduction of opposing magnet reaction MMF. This increases sleeve-induced eddy-current density and loss, resulting in an increase in total rotor loss. Coupled with this, there is a reduction in the shielding effect of the magnet's eddy currents, resulting in increased shaft loss. This is most evident for the two pole field that is now able to penetrate deep into the shaft.

A greater number of segments per pole further reduce magnet loss, however, shaft and sleeve eddy-current loss is able to increase further still. The limiting case can be seen when considering magnets with zero conductivity.
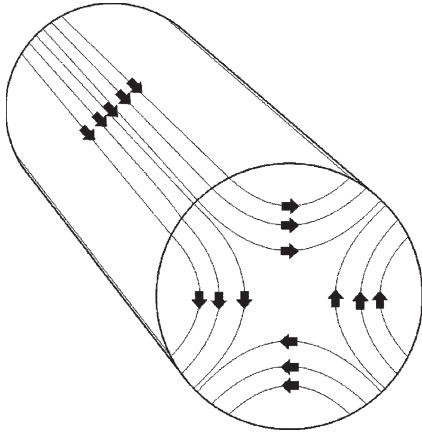
Fig. 13.   Eddy-current path in a solid rotor [18].

TABLE V
2-D FE CALCULATED LOSSES USING THE HARMONIC METHOD
WITH END CORRECTION ADDED

Harmonic	Rotor eddy current loss (W)	
	2D harmonic model without end correction	2D harmonic model with end correction
1st	4499	6300
5th	869	812
7th and higher	616	594
Total Loss	5984	7706

In order to benefit from a reduction in total loss via magnet segmentation, the reduction of loss in the magnets must counteract the increased loss in the sleeve and shaft. This only occurs with a large number of segments per pole and is limited to a 5% reduction in loss when considering the air-gap harmonic spectrum in Fig. 6.

F. 3-D Solid Rotor Effects

The previous models discussed are in two dimensions only. In reality, the extra path length that the circulating eddy-currents must follow at the ends of the rotor must be taken into account. This is illustrated in Fig. 13.

The ratio of eddy-current axial path length to eddy-current rotor end path length is dependent on the order of the harmonic.

With the lower order harmonics, the air-gap length is a small part of the overall flux path, and hence, the rotor eddy currents are able to develop somewhere near ampere turn reflection. This is commonly described as "current forced." Under these circumstances, the extra path length for the eddy currents (i.e., up to 40%) has little effect on their magnitude, and hence, extra end region path length increases the loss.

On the other hand, for the higher order harmonics, the air-gap length is a far larger portion of the total flux path length, and hence, full ampere turn reflection does not develop despite the higher frequency. This voltage forced situation means that this extra end region path length significantly reduces the size of the eddy currents and, hence, reduces their loss.

Table V summarizes the change resulting from the various harmonics when this path length adjustment is used [18]. In this, the increased loss due to the current forced two-pole eddy-current and the decreased loss due to the voltage forced

higher order eddy currents is evident. For verification, a full 3-D nonlinear moving rotor time-step FE model was created. Four days of computation time was required to simulate a single load condition. The total rotor loss was found to be 7540 W. By comparison, the 2-D harmonic result with the empirical factor added gave a total rotor loss of 7706 W, which gives a 2% difference. This only required a few seconds of computation.

The harmonic method allows the effect of the end of the rotor to be added easily for each harmonic separately, whereas if the time-stepping method were used, the loss due to each harmonic and the different effects of the low- and high-order harmonics could not be appreciated.

It was concluded that with 2-D time-stepping, an end effect correction could not be added. If the effect of the end of the rotor was required and time-stepping deemed necessary, a full 3-D model would need to be constructed, and as discussed earlier, a single solution would take several days to solve.

VII. CONCLUSION

Increasing the physical size of fault-tolerant machines to achieve a 100-kW power level has resulted in a reduction in efficiency and a change in the balance of machine losses, with rotor eddy-current loss becoming the dominant loss mechanism. To achieve a more acceptable level of efficiency, rotor eddy-current loss is first investigated. To do this, a method of calculating rotor eddy-current loss, which is both accurate and yields rapid results, is required to investigate the effect design modifications have.

Full knowledge of the time-varying magnetic field distribution within a machine requires the use of 3-D time-stepping FE methods, with movement incorporated into the mesh. During the investigative stage of a machine design, such an approach is very inconvenient, as a single solution may take several days to solve.

Another approach is to use a 2-D time-stepped model. Such a model will give a solution within the hour; however, care must be taken in its construction, as the results gained may be inaccurate due to discretization limitations and the difficulty of accounting for end effects. Investigation of design changes will also require a new mesh and solution.

An alternative approach is to use a harmonic method. Using a harmonic approach in calculating rotor eddy-current loss allows the designer to see which harmonics are causing the majority of the loss and take appropriate action. Knowing that a certain harmonic is causing the majority of the loss allows investigation into what changes can be made to the machine design, such as changing the tooth span and slot opening size. By recalculating the air-gap Fourier series and applying this result to a set of precalculated 2-D FE results, the effect of such a change on the machine design can be rapidly seen. The effects of the rotor end region can be added using the adjustment factor well known from solid rotor induction machines, and again, the result can be rapidly seen without the need to build a 3-D FE model. Having the ability to analyze changes to the design of a machine in such a way is of great benefit to the designer and will allow faster development toward a final design. What is being ignored is

proper account of saturation, but this has been shown to be only a small factor in the results.

Rotor eddy-current, no-load, and winding losses cannot be treated in isolation, as modifying the machine design to reduce loss due to one often results in increasing loss due to the others. Changing the stator design has reduced rotor eddy current loss by decreasing the magnitude of the loss inducing fifth harmonic. Increasing the air-gap length by reducing the rotor radius has reduced rotor eddy current loss due to the high-order air-gap harmonics and no-load loss, as viscous drag loss is most heavily dependent on the rotor radius. However, this has reduced the magnetic loading and the output torque of the machine. The torque level is restored by increasing the electrical loading, which increases winding loss. Winding loss is then reduced by using a multistrand conductor.

Overall, a reduction in calculated loss of 5.7 kW is achieved when compared to the original 100-kW machine design. The final design is now under construction.

Acknowledgment

References

[1] E. Richter, "Switched reluctance machines for high performance operations in a harsh environment—A review paper," in *Proc. ICEM Conf.*, Boston, MA, 1990, pp. 18–24.

[2] T. J. E. Miller, "Faults and unbalanced forces in the switched reluctance machine," *IEEE Trans. Ind. Appl.*, vol. 31, no. 2, pp. 319–328, Mar./Apr. 1995.

[3] A. G. Jack, B. C. Mecrow, and J. A. Haylock, "A comparative study of permanent magnet and switched reluctance motors for high performance fault tolerant applications," *IEEE Trans. Ind. Appl.*, vol. 32, no. 4, pp. 889–895, Jul./Aug. 1996.

[4] A. G. Jack and B. C. Mecrow, "Safety critical drives for aerospace applications," in *Proc. ICEM Conf.*, Paris, France, 1994, vol. 1, pp. 91–96.

[5] T. M. Jahns, "Improved reliability in solid state AC drives by means of multiple independent phase-drive units," *IEEE Trans Ind. Appl.*, vol. IA-16, no. 3, pp. 321–331, May 1980.

[6] B. C. Mecrow, A. G. Jack, and J. A. Haylock, "Fault tolerant permanent magnet machine drives," *Proc. Inst. Electr. Eng.*, vol. 143, no. 6, pt. B5, pp. 437–442, Nov. 1996.

[7] J. A. Haylock, B. C. Mecrow, A. G. Jack, and D. J. Atkinson, "On-line detection of winding short-circuits in inverter fed drives," in *Proc. 9th Int. Conf. EMD*, Canterbury, U.K., Sep. 1–3, 1999, pp. 258–262.

[8] ——, "Operation of fault tolerant machines with winding failures," in *Proc. IEEE Int. Electr. Mach. and Drives Conf.*, 1997, pp. MC3/10.1–MC3/10.3.

[9] S. Nandi and H. A. Toliyat, "Fault diagnosis of electrical machines—A review," in *Proc. IEEE Int. Electr. Mach. and Drives Conf.*, 1999, pp. 219–221.

[10] T. Gopalarathnam, H. A. Toliyat, and J. C. Moreira, "Multi-phase fault-tolerant brushless DC motor drives," in *Conf. Rec. IEEE-IAS Annu. Meeting*, 2000, pp. 1683–1688. Part vol. 3.

[11] B. A. Welchko, T. A. Lipo, T. M. Jahns, and S. E. Schulz, "Fault tolerant three phase AC motor drive topologies: A comparison of features, cost and limitations," *IEEE Trans. Power Electron.*, vol. 19, no. 4, pp. 1108–1116, Jul. 2004.

[12] B. C. Mecrow, A. G. Jack, D. J. Atkinson, S. Green, G. J. Atkinson, A. King, and B. Green, "Design and testing of a 4 phase fault tolerant permanent magnet machine for an engine fuel pump," *IEEE Trans. Energy Convers.*, vol. 19, no. 4, pp. 671–678, Dec. 2004.

[13] G. J. Atkinson, B. C. Mecrow, A. G. Jack, D. J. Atkinson, and B. Green, "The influence of stator design on the performance of fault tolerant machines," in *Proc. 16th ICEM Conf.*, Krakow, Poland, 2004, pp. 227–228.

[14] E. Bilgen and R. Boulos, "Functional dependence of torque coefficient of coaxial cylinders on gap width and Reynolds numbers," *Trans. ASME, J. Fluids Eng.*, vol. 95, pp. 122–126, Mar. 1973.

[15] K. Atallah, D. Howe, P. H. Mellor, and D. A. Stone, "Rotor loss in permanent-magnet brushless AC machines," *IEEE Trans. Ind. Appl.*, vol. 36, no. 6, pp. 1612–1617, Nov./Dec. 2000.

[16] H. Toda, Z. Xia, J. Wang, K. Atallah, and D. Howe, "Rotor eddy-current loss in permanent magnet brushless machines," *IEEE Trans. Magn.*, vol. 40, no. 4, pp. 2104–2106, Jul. 2004.

[17] J. D. Ede, K. Atallah, J. Wang, and D. Howe, "Effect of optimal torque control on rotor loss of fault-tolerant permanent magnet brushless machines," *IEEE Trans. Magn.*, vol. 38, no. 5, pp. 3291–3293, Sep. 2002.

[18] H. Yee, "Effects of finite length in solid rotor induction machines," *Proc. Inst. Electr. Eng.*, vol. 118, no. 8, pp. 1025–1033, 1971.

Glynn J. Atkinson (M'03) received the Master's degree in electrical and electronic engineering in 2001 from the University of Newcastle upon Tyne, Newcastle upon Tyne, U.K., where he is currently working toward the Engineering Doctorate degree.

He is currently doing research on the design of fault-tolerant machines for use in aerospace applications.

Barrie C. Mecrow (M'92) received the Ph.D. degree from the University of Newcastle upon Tyne, Newcastle upon Tyne, U.K. His Ph.D. research was on three-dimensional eddy-current computation applied to turbogenerators.

He was a turbogenerator Design Engineer with NEI Parsons, Newcastle upon Tyne, U.K., until 1987. He became a Lecturer at the University of Newcastle upon Tyne, in 1987, where he is currently a Professor of electrical power engineering. He is involved in a range of research projects, including fault-tolerant drives, high-performance permanent-magnet machines, and novel switched reluctance drives.

Alan G. Jack (M'00) received the Ph.D. degree from Southampton University, Southampton, U.K., in 1975 for his work on numerical analysis of electromagnetic fields in turbogenerators.

He holds the department's Chair in electrical engineering, is a past Head of department, and is the Leader of the Newcastle Electric Drives and Machines Group. He is the author of over 80 papers in the area of electrical machines and drives. He has been with the University of Newcastle upon Tyne, Newcastle upon Tyne, U.K., for over 20 years, joining them from NEI Parsons, who he was with for 13 years with roles from Craft Apprentice to Principal Design Engineer.

David J. Atkinson received the Ph.D. degree from the University of Newcastle upon Tyne, Newcastle upon Tyne, U.K., for his research on the use of Kalman-filter-based estimation on induction motor vector-controlled drives.

He is currently a Senior Lecturer with the Drives and Machines Group, University of Newcastle upon Tyne. His research interests include electrical drive systems, real-time estimation and control, power electronics, and wind power generation. Current research project involvement includes sensorless vector drives, fault-tolerant drives, and cascade induction generators. Prior to his university appointment in 1987, he had spent 17 years in the industry.

Maamar Benarous received the M.Eng. degree from the University of Bab-el-zouar Algiers, Algiers, Algeria, in 1989, and the Ph.D. degree in electrical engineering from the University of Bath, Bath, U.K., in 1997.

He is currently with the Electromagnetic Systems Technical Centre, Goodrich Corporation, Birmingham, U.K., as an Engineering Consultant. His interests cover the fields of rotating and linear machine design and analysis for aerospace applications.

Parminder Sangha received the B.Sc. degree in electrical engineering from the University of Newcastle upon Tyne, Newcastle upon Tyne, U.K., and the Ph.D. degree from the University of Bath, Bath, U.K.

He is currently the R&D Manager of the Electromagnetic Systems Technical Centre, Goodrich Corporation, Birmingham, U.K. His main interests are in the design/development of electric actuation devices and numerical analysis techniques.